ACS APPLIED MATERIALS & INTERFACES

Research Article

www.acsami.org

Potential Tuning of Nanoarchitectures Based on Phthalocyanine Nanopillars: Construction of Effective Photocurrent Generation Systems

Takuya Kawaguchi,[†] Shota Okamura,[†] Takanari Togashi,[†] Wataru Harada,[†] Mana Hirahara,[†] Ryosuke Miyake,[‡] Masa-aki Haga,[§] Takao Ishida,[∥] Masato Kurihara,*[,†] and Katsuhiko Kanaizuka*[,†]

[†]Department of Material and Biological Chemistry, Faculty of Science, Yamagata University, 1-4-12 Kojirakawa-machi, Yamagata 990-8560, Japan

[‡]Department of Chemistry, Graduate School of Humanities and Science, Ochanomizu University, 2-1-1 Otsuka, Bunkyo-ku, Tokyo 112-8610, Japan

[§]Department of Applied Chemistry, Faculty of Science and Engineering, Chuo University, 1-13-27 Kasuga, Bunkyo-ku, Tokyo 112-8551, Japan

[∥]Nanosystem Research Institute, National Institute of Advanced Industrial Science and Technology, 1-2-1 Namiki, Tsukuba, Ibaraki 305-8564, Japan

Supporting Information

ABSTRACT: Nanopillars composed of a photoresponsive phthalocyanine derivative have been conveniently fabricated using a continuous silane coupling reaction on a substrate. The chemical potentials of phthalocyanine nanopillars (PNs) are precisely controlled by changing the number of phthalocyanine derivatives on the substrate. In addition, photocurrent generation efficiencies have been strongly influenced by the number of phthalocyanine derivatives. High photocurrent conversion cells in a solid state have been obtained by the combination of PNs and a fullerene derivative.

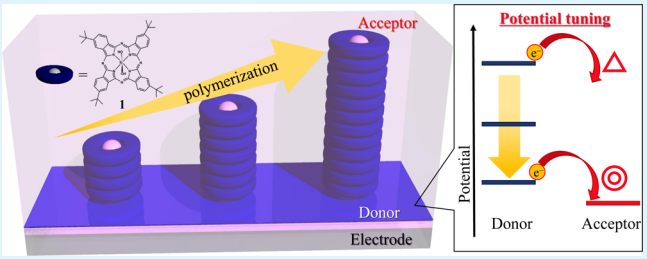

KEYWORDS: *phthalocyanine, nanoarchitecture, silane coupling reaction, photocurrent, potential tuning*

INTRODUCTION

The design of an electrode surface with nanoarchitectures composed of functional molecules via a convenient fabrication method has been a key research topic regarding the development of chemical devices.[1] Specifically, electrodes modified with photoresponsive and/or redox-active materials show unique photophysical properties; therefore, these devices have been used as high-performance photocurrent conversion cells, organic light-emitting diodes, catalytic devices, fuel cells, and so on.[2,3] In order to construct uniform films or nanoarchitectures of functional molecules on substrates, a layer-by-layer molecular fabrication method in a solution, a spin-coating method, and electropolymerization have been widely used to date.[4−6] By using these methods, not only homogeneous but also heterogeneous films can be easily constructed. As a result, the direction of electron and/or hole transfer can be precisely controlled in the potential controlled bilayer films. Abruna and Murray have developed the construction of redox-active bilayer films, and the diode effect of these films has been clarified.[7−9] Many researchers have constructed three-dimensional nanoarchitectures by the combination of metal ions and a bridging ligand.[10−15] We have also reported on the construction of highly oriented nanoarchitectures [from one- to three-dimensional (3D) architectures] using step-by-step molecular fabrication methods.[5,16] However, the construction of oriented nanoarchitectures is sometimes time-consuming work, and, furthermore, the chemical potential of these nanoarchitectures does not change from that of the starting materials in previous cases.

Recently, we developed the construction of an uneven film (nano-bamboo-shoot structures) composed of porphyrin derivatives via a one-pot spontaneous silane coupling reaction.[17,18] A silane coupling reaction has been widely used for the construction of 3D materials and devices.[19−25] By using this immersion method, functional molecules are easily assembled on an electrode, and uneven surfaces can be formed in a few hours. This convenient molecular fabrication technique is also appropriate for functional bulky (huge) molecules [for example, a tris(bipyridine)ruthenium(II) complex-combined porphyrin molecule]. The electronic states of porphyrin assemblies are often similar to those of a porphyrin monomer.[26−28]

Received: May 29, 2015
Accepted: July 29, 2015
Published: August 19, 2015

DOI: 10.1021/acsami.5b04646
ACS Appl. Mater. Interfaces 2015, 7, 19098−19103

We have considered that control of not only the shape of the assembled molecules but also their chemical potentials is important for the creation of intriguing chemical devices. In order to obtain an effective photoinduced electron-transfer system, the precise tuning of the energy levels of the highest occupied molecular orbital (HOMO) and lowest unoccupied molecular orbital of a donor and acceptor is quite important.[29,30] From these viewpoints, we have employed a π-extended molecule[31] such as phthalocyanine in this study. Phthalocyanine, having a reactive group, makes a stacked structure in a solid state, and the electronic state of the stacked structure is different from that of a monomer.[32,33] This indicates that the electronic state of the assembled architecture can be controlled by tuning the number of stacked molecules, and we have attempted to construct the assembled architecture on an electrode. Figure 1 shows our new concept for the

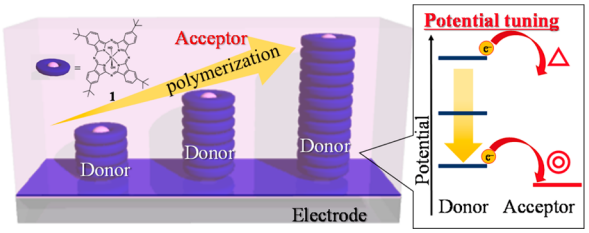

Figure 1. Concept for the construction of potential tunable nanoarchitectures. Creation of an effective photoinduced electron-transfer system on a substrate.

construction of a potential tunable nanoarchitecture using a phthalocyanine derivative on a substrate. Herein, we report on the one-pot spontaneous polymerization of a phthalocyanine derivative using a silane coupling reaction that forms nanopillars on an electrode. It should be noted that the chemical potential of the nanopillars can be precisely controlled. As a result, the photocurrent generation efficiency of the phthalocyanine nanopillars (PNs) can also be controlled.

EXPERIMENTAL SECTION

Materials. Reagents of silicon 2,9,16,23-tetra-*tert*-butyl-29*H*,31*H*-phthalocyanine dihydroxide (**1**) and [6,6]-phenyl C_{61} butyric acid methyl ester (PCBM) were purchased from Sigma-Aldrich; $SiCl_4$ was purchased from TCI. Na_2SO_4 was purchased from Kanto Chemicals. These reagents were used without further purification. A glass (20 mm × 20 mm) and indium–tin oxide (ITO; 10 Ω/cm^2, Furuuchi Kagaku) were washed with 2-propanol, methanol, and then pure water before use. Organic solvents were purchased from Kanto Chemicals. Aluminum wire (⌀ = 2.0 mm) was purchased from Nilaco.

Methods. Atomic force microscopy (AFM) images were observed using a Shimadzu SPM-9600 atomic force microscope. UV–vis absorption spectra were monitored using a Shimadzu UV-3150 spectrometer. Cyclic voltammetry (CV) of **1** and PNs on ITO was measured in a 0.1 M tetrabutylammonium hexafluorophosphate ($TBAPF_4$) solution in CH_2Cl_2 using an ALS model 660A electrochemical analyzer. Photoelectrochemical measurement was carried out in a 0.1 M Na_2SO_4 aqueous solution under various potentials. PCBM was fixed by using a spin coater (KYOWARIKEN K-359S1). For the construction of a solid cell, aluminum was deposited on films using a ULVAC KIKO Inc. VPC-260F instrument, and the thickness of aluminum was 80 nm.

Epitaxial Formation of PNs on Substrates. A small excess amount of $SiCl_4$ was added to a 0.1 mM chloroform solution containing **1** at room temperature in the atmosphere. A glass or ITO substrate was immersed in the solution mixture for various periods of time. The plate was thoroughly washed by ultrasonic cleaning for 1 min in order to remove the physically attached molecules, and then it was dried by a stream of nitrogen gas.

Preparation of Films Composed of ITO/PNs/PCBM. A 1.0 mM PCBM solution of chloroform (0.25 mL) was spin-coated (1000 rpm for 5 s and then 1500 rpm for 10 s) on a plate with PNs and then heated at 100 °C for 1 h.

RESULTS AND DISCUSSION

Epitaxial Formation of PNs on Substrates. UV–vis absorption spectra of glass plates after immersion in a mixed solution of **1** and $SiCl_4$ for 10, 30, and 60 min are shown in Figure 2 (these films are defined as 10, 30, and 60 min PNs,

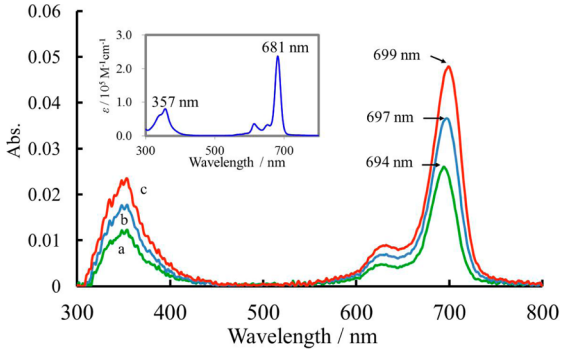

Figure 2. UV–vis absorption spectra of (a) 10, (b) 30, and (c) 60 min PNs on glass substrates. Inset: UV–vis absorption spectrum of **1** in chloroform at room temperature.

respectively). The inset in Figure 2 shows the electronic spectrum of **1** in a chloroform solution, and two intense peaks were observed at 357 and 681 nm. These absorptions are based on the Soret and Q bands of a typical phthalocyanine, respectively. These peaks were red-shifted with longer immersion time. For example, the Q bands were observed at 694 nm in the 10 min PNs and at 699 nm in the 60 min PNs. The expanded electronic spectra are shown in Figure S1a. This behavior was not observed when porphyrin derivatives were used.[17,18] We consider this red shift to be based on the electronic interaction among intra- and interwires.[34,35] This result indicates that electron- and/or hole-transfer networks are formed in a polymer; PN structure probably shows high electron- and/or hole-transport ability. Saeki has reported the high hole-transfer mobility of wired (polymerized) phthalocyanine derivatives.[32,36] The number of phthalocyanines in ITO/120 min PNs was roughly calculated (because of the red shift of Q bands) using absorbance of the films and a molar extinction coefficient in solution of 1.5 × 10^{-9} mol/cm^2. Elemental analysis (X-ray photoelectron spectroscopy) of the surface also supports the fixation of a phthalocyanine derivative (shown in Figure S2). Electronic spectra of ITO, ITO/PCBM, and ITO/120 min PNs/PCBM are also shown in Figure S3. The prepared PN structure is stable because nanopillars are obtained by AFM after the PNs/PCBM are washed with chloroform.

Electrochemical Behavior of 1 and PNs. Cyclic voltammograms of **1** in solution and 120 min PNs on ITO are shown in Figure 3. Reversible two-step, one-electron reduction ($E^{\circ\prime}$ = −0.96 and −1.39 V vs Ag/Ag$^+$) and reversible ($E^{\circ\prime}$ = 0.60 V) and multistep irreversible oxidation (E_{pa} = 0.87 and 1.38 V) waves were observed in compound **1** in solution (see Figure 3a). After the formation of a PN on ITO, a broad oxidation wave was observed at 0.67 V vs Ag/AgCl (see Figure

DOI: 10.1021/acsami.5b04646
ACS Appl. Mater. Interfaces 2015, 7, 19098–19103

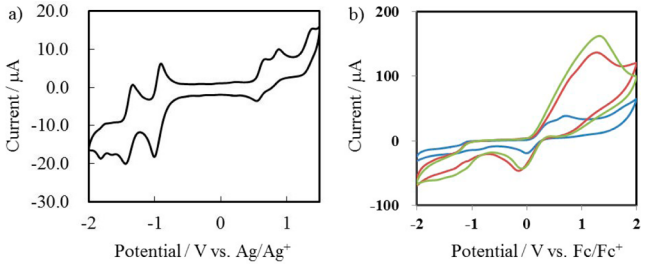

Figure 3. Cyclic voltammograms of (a) **1** in 0.1 M $TBAPF_4/CH_2Cl_2$ at a scan rate of 0.1 V/s and (b) 5 min PNs (blue), 15 min PNs (red), and 60 min PNs (green) on ITO electrodes in 0.1 M $TBAPF_4/CH_2Cl_2$ at a scan rate of 0.1 V/s.

3b). The expanded voltammograms are shown in Figure S1b. The anodic area was increased with an increase of the immersion time, indicating polymer formation on the electrode. Furthermore, the broadening of the wave indicates that the ohmic component of phthalocyanine is also included. It should be noted that the potential of HOMO (oxidation wave) is gradually shifted upon polymerization. The cyclic voltammogram of PCBM in a solution is shown in Figure S4. These redox potentials obtained by CV and the literature[37−40] were used for the description of energy diagrams.

Morphology of PNs on Substrates. The epitaxial growth of PNs was monitored by AFM. Figure 4 shows AFM images of 10, 30, and 60 min PNs on a glass plate. The number of white dots increased with an increase in the immersion time. The average height of the dots was estimated to be 25 nm on glass and 20 nm on ITO, which is higher than that of the porphyrin system (ca. 7 nm). This indicates that the speed of epitaxial growth in a solution depends on the size of molecule (solubility) and/or the manner of $\pi-\pi$ interaction among molecules. After depositition of PCBM on PNs, an image of the flat surface was observed (shown in Figure S3).

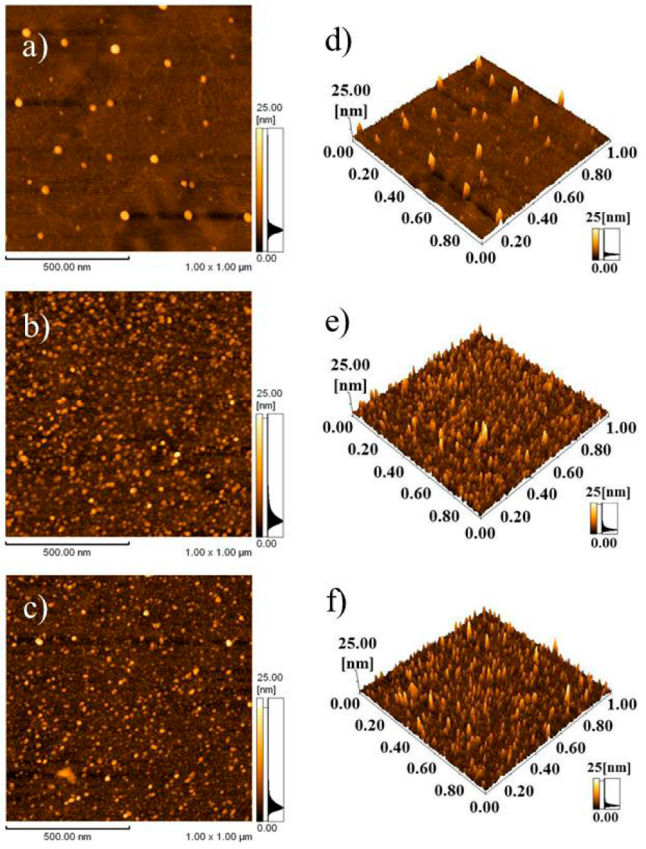

Figure 4. AFM images of 10 min PNs [top view (a) and 3D view (d)], 30 min PNs [top view (b) and 3D view (e)], and 60 min PNs [top view (c) and 3D view (f)].

Photocurrent Generation of PNs in a Solution. Photocurrent measurements of PNs of various immersion times were carried out in a 0.1 M Na_2SO_4 aqueous solution with or without oxygen molecules (an image of the cell is shown in Figure 5a). In order to determine the stability of the

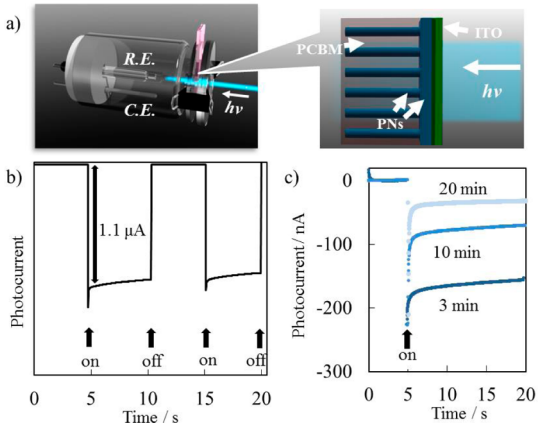

Figure 5. (a) Image of a cell of photocurrent generation. (b) On−off responses of photocurrent upon light irradiation of 120 min PNs/PCBM at 686 nm in a 0.1 M Na_2SO_4 aqueous solution at −0.5 V vs Ag/AgCl. (c) Photocurrent generation after nitrogen bubbling for 3, 10, and 20 min.

PNs on ITO, on−off responses of the film of 120 min PNs/PCBM were measured. The number of PCBM was calculated using absorbance of the films and a molar extinction coefficient in solution of 5.1×10^{-9} mol/cm^2. As shown in Figure 5b, stable cathodic photocurrents were observed upon light irradiation (λ_{ex} = 686 nm). In order to clarify the mechanism of the photocurrent, the effect of oxygen molecules on the photocurrent generation was examined. The photocurrent responses of 120 min PNs/PCBM before and after nitrogen bubbling are shown in Figure 5c. The photocurrent was reduced via nitrogen bubbling; therefore, the oxygen molecules in the solution acted as an electron acceptor. No photocurrent was observed in the ITO/PNs system, indicating fast back-electron transfer from O_2^- to PNs. The red line in Figure 6a shows a plot of the photocurrent generation quantum yield versus wavelength in 5 min PNs/PCBM. The action spectra are nicely fitted to the absorption spectra of PNs/PCBM, indicating that triggers of photocurrent generation are both PCBM and PNs. On the basis of these results, the electron-transfer mechanism upon light irradiation is described in Figure 7. In the region of 400−600 nm, PCBM acted as a trigger of photocurrent generation, and PNs acted as an electron donor for PCBM (PCBM to oxygen, PNs to PCBM, and ITO to PNs). On the other hand, in the region of 600−800 nm, PNs acted as a trigger of photocurrent generation, and PCBM acted as an electron acceptor for PNs (PNs to PCBM, ITO to PNs, and PCBM to oxygen). This penetrating PNs/PCBM device showed much higher photocurrent generation than the spin-

DOI: 10.1021/acsami.5b04646
ACS Appl. Mater. Interfaces 2015, 7, 19098−19103

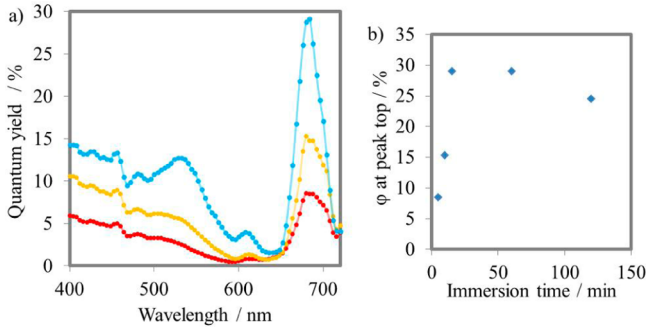

Figure 6. (a) Photocurrent quantum yields at various wavelengths in 5 min PNs/PCBM (red), 10 min PNs/PCBM (yellow), and 15 min PNs/PCBM (blue). (b) Plots of maximum quantum yields versus immersion time.

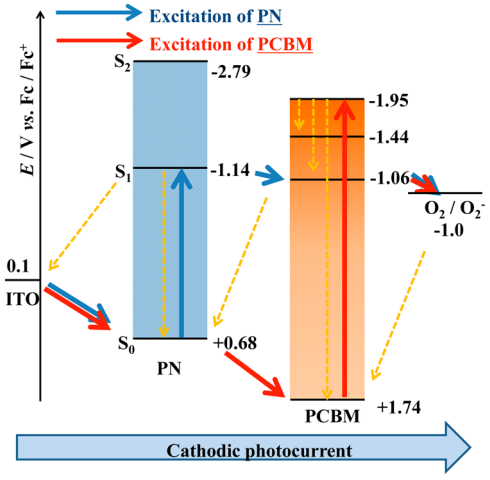

Figure 7. Plausible mechanism of cathodic photocurrent generation in an PNs/PCBM/oxygen cell. Red arrows are the direction of current flow upon excitation of PCBM, and blue arrows are the direction of current flow upon excitation of PNs.

coating device (ITO/**1**/PCBM; see the blue dotted line in Figure S5).

One of the important subjects for photocurrent generation is tuning the energy level of molecular architectures. Our convenient molecular epitaxial growth method in solution makes the potential tuning possible. As we described in the sessions of electronic spectra and CVs, the energy level of PNs depends on the immersion time (the number of molecules). In order to clarify the effect of the number of phthalocyanines, photocurrent generation efficiencies of 5, 10, and 15 min PNs/PCBM are shown in Figure 6a. The efficiency increased with an increase in the immersion time. We consider that the electron injection efficiency from PNs bearing a wide valence band (based on HOMO of **1**) to PCBM was increased (see Figure S1c). Furthermore, quantum yields at 500−550 nm also increased with longer immersion time. This is probably because of the formation of charge-transfer complexes among PNs and PCBM. Plots of the peak efficiency versus immersion time are shown in Figure 6b. It should be noted that the plots were bent over with longer immersion time. These results indicate that the tuning of the energy levels is important for the construction of a photocurrent generation system, and our concept for a potential tunable nanoarchitecture has the potential for the creation of smart chemical devices.

Photocurrent Generation of Solid Cells. In the next step, we constructed solvent-free photocurrent conversion cells (an image is shown in Figure S6) using uneven structures.[41−45] Aluminum was deposited on the PNs/PCBM, and a gold wire was fixed on the aluminum using gold paste. The spectrum of the external quantum efficiency of the 120 min PNs/PCBM/Al cell was measured; a photocurrent action spectrum (Figure 8)

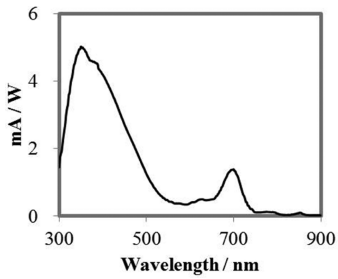

Figure 8. Spectrum of the external quantum efficiency at various wavelengths in the ITO/120 min PNs/PCBM/Al cell.

was nicely fitted to the absorption spectra (Figure S3), indicating that the triggers of photocurrent generation are both PCBM and PNs, similar to the solution system. A current−voltage curve in the 120 min PNs/PCBM/Al cell is shown in Figure S6. These results indicate that solvent-free photocurrent conversion cells can be constructed.

CONCLUSION

We have conveniently constructed PNs via wet-process epitaxial growth on a substrate. The number of phthalocyanines on a substrate can be easily controlled by the period of immersion time. The mixed structure of PNs and PCBM shows a stable cathodic photocurrent, and the efficiency of photocurrent generation was controlled via a change in the number of phthalocyanine derivatives. These new concepts for tuning the energy levels on nanoarchitectures will open new fields of chemical devices such as high-performance organic solar cells.

ASSOCIATED CONTENT

Supporting Information

The Supporting Information is available free of charge on the ACS Publications website at DOI: 10.1021/acsami.5b04646.

Description of the material (PDF)

AUTHOR INFORMATION

Corresponding Authors

*E-mail: kurihara@sci.kj.yamagata-u.ac.jp.
*E-mail: kanaizuka@sci.kj.yamagata-u.ac.jp.

Notes

The authors declare no competing financial interest.

ACKNOWLEDGMENTS

This work was supported by Dissemination of Tenure Tracking System Program of Ministry of Education, Culture, Sports, Science and Technology, Japan.

REFERENCES

(1) Nishihara, H. Coordination Programming: A New Concept for the Creation of Multi Functional Molecular Systems. *Chem. Lett.* **2014**, *43*, 388−395.

DOI: 10.1021/acsami.5b04646
ACS Appl. Mater. Interfaces 2015, 7, 19098−19103

(2) Joachim, C.; Gimzewski, J. K.; Aviram, A. Electronics Using Hybrid-Molecular and Mono-Molecular Devices. *Nature* **2000**, *408*, 541−548.
(3) Kaltenbrunner, M.; White, M. S.; Głowacki, E. D.; Sekitani, T.; Someya, T.; Sariciftci, N. S.; Bauer, S. Ultrathin and Lightweight Organic Solar Cells with High Flexibility. *Nat. Commun.* **2012**, *3*, 770−776.
(4) Ulman, A. Formation and Structure of Self-Assembled Monolayers. *Chem. Rev.* **1996**, *96*, 1533−1554.
(5) Kanaizuka, K.; Murata, M.; Nishimori, Y.; Mori, I.; Nishio, K.; Masuda, H.; Nishihara, H. Stepwise Preparation of Linear π-conjugated Bis(terpyridine)metal Polymer Chains at Gold Surface. *Chem. Lett.* **2005**, *34*, 534−535.
(6) Zhong, Y.-W.; Yao, C.-J.; Nie, H.-J. Electropolymerized of Vinyl-Substituted Complexes: Synthesis, Characterization, and Applications. *Coord. Chem. Rev.* **2013**, *257*, 1357−1372.
(7) Abruna, H. D.; Denisevich, P.; Umana, M.; Meyer, T. J.; Murray, R. W. Rectifying Interfaces Using Two-Layer Films of Electrochemically Polymerized Vinylpyridine and Vinylbipyridine Complexs of Ruthenium and Iron on Electrodes. *J. Am. Chem. Soc.* **1981**, *103*, 1−5.
(8) Denisevich, P.; Willman, K. W.; Murray, R. W. Unidirectional Current Flow and Charge State Trapping at Redox Polymer Interfaces on Bilayer Electrodes: Principles, Experimental Demonstration, and Theory. *J. Am. Chem. Soc.* **1981**, *103*, 4727−4737.
(9) Abruna, H. D. Coordination Chemistry in Two Dimensions: Chemically Modified Electrodes. *Coord. Chem. Rev.* **1988**, *86*, 135−189.
(10) Biemmi, E.; Scherb, C.; Bein, T. Oriented Growth of the Metal Organic Framework $Cu_3(BTC)_2(H_2O)_3{\cdot}xH_2O$ Tunable with Functionalized Self-Assembled Monolayers. *J. Am. Chem. Soc.* **2007**, *129*, 8054−8055.
(11) Hermes, S.; Schröder, F.; Chelmowski, R.; Wöll, C.; Fischer, R. A. Selective Nucleation and Growth of Metal-Organic Framework Thin Films on patterned $COOH/CF_3$-Terminated Self-Assembled Monolayers on Au(111). *J. Am. Chem. Soc.* **2005**, *127*, 13744−13745.
(12) Shekhah, O.; Wang, H.; Kowarik, S.; Schreiber, F.; Paulus, M.; Tolan, M.; Sternemann, C.; Evers, F.; Zacher, D.; Fischer, R. A.; Wöll, C. Step-by-Step Route for the Synthesis of Metal-Organic Frameworks. *J. Am. Chem. Soc.* **2007**, *129*, 15118−15119.
(13) So, M. C.; Jin, S.; Son, H.-J.; Wiederrecht, G. P.; Farha, O. K.; Hupp, J. T. Layer-by-Layer Fabrication of Oriented Porous Thin Films Based on Porphyrin-Containing Metal-Organic Frameworks. *J. Am. Chem. Soc.* **2013**, *135*, 15698−15701.
(14) Shekhah, O.; Wang, H.; Paradinas, M.; Ocal, C.; Schüpbach, B.; Terfort, A.; Zacher, D.; Fischer, R. A.; Wöll, C. Controlling Interpenetration in Metal-Organic Framework by Liquid-Phase Epitaxy. *Nat. Mater.* **2009**, *8*, 481−484.
(15) Falcaro, P.; Ricco, R.; Doherty, C. M.; Liang, K.; Hill, A. J.; Styles, M. J. MOF Positioning Technology and Device Fabrication. *Chem. Soc. Rev.* **2014**, *43*, 5513−5560.
(16) Kanaizuka, K.; Haruki, R.; Sakata, O.; Yoshimoto, M.; Akita, Y.; Kitagawa, H. Constructio of Highly Orieted Crystalline Surface Coordination Polymers Composed of Copper Dithiooxamide Complexes. *J. Am. Chem. Soc.* **2008**, *130*, 15778−15779.
(17) Kanaizuka, K.; Izumi, A.; Ishizaki, M.; Kon, H.; Togashi, T.; Miyake, R.; Ishida, T.; Tamura, R.; Haga, M.; Moritani, Y.; Sakamoto, M.; Kurihara, M. Molecular Nanostamp Based on One-Dimensional Porphyrin Polymers. *ACS Appl. Mater. Interfaces* **2013**, *5*, 6879−6885.
(18) Togashi, T.; Izumi, A.; Kon, H.; Kanaizuka, K.; Ishizaki, M.; Miyake, R.; Chang, H.-C.; Haga, M.; Sakamoto, M.; Kurihara, M. Stpontaneous Constructution of Nanoneedles Using Rythenium Complex-conjugated Porphyrins on Substrates. *Chem. Lett.* **2014**, *43*, 1201−1203.
(19) Peng, H.; Lu, Y. Squarely Mesoporous and Functional Nanocomposites by Self-Directed Assembly of Organosilane. *Adv. Mater.* **2008**, *20*, 797−800.
(20) Li, Y.; Auras, F.; Löbermann, F.; Döblinger, M.; Schuster, J.; Peter, L.; Trauner, D.; Bein, T. A Photoactive Porphyrin-Based Periodic Mesoporous Organosilica Thin Film. *J. Am. Chem. Soc.* **2013**, *135*, 18513−18519.
(21) Mizoshita, N.; Tani, T.; Inagaki, S. Highly Conductive Organisilica Hybrid Films Prepared from a Liquid-Crystal Perylene Bisimide Precursor. *Adv. Funct. Mater.* **2011**, *21*, 3291−3296.
(22) Sayari, A.; Wang, W. Molecularly Ordered Nanoporous Organisilicates Prepared with and without Surfactants. *J. Am. Chem. Soc.* **2005**, *127*, 12194−12195.
(23) Minoofar, P. N.; Hernandez, R.; Chia, S.; Dunn, B.; Zink, J. I.; Franville, A.-C. Placement and Chracterization of pairs of Luminescent Molecules in Spatially Separated Regions of Nanostructured Thin Films. *J. Am. Chem. Soc.* **2002**, *124*, 14388−14396.
(24) Mizoshita, N.; Ikai, M.; Tani, T.; Inagaki, S. hole-Transporting Periodic Mesostructured. *J. Am. Chem. Soc.* **2009**, *131*, 14225−14227.
(25) Brinker, C. J.; Lu, Y.; Sellinger, A.; Fan, H. Evaporation-Induced Self Assembly: Nanostructures Made Easy. *Adv. Mater.* **1999**, *11*, 579−585.
(26) Lee, D.-C.; Morales, G. M.; Lee, Y.; Yu, L. Cofacial Porphyrin Multilayers via Layer-by-Layer Assembly. *Chem. Commun.* **2006**, *42*, 100−102.
(27) Sakai, N.; Bhosale, R.; Emery, D.; Mareda, J.; Matile, S. Supramolecular n/p-Heterojunction Photosystems with Anitiparallel Redox Gradients in Electron- and Hole- Transporting Pathways. *J. Am. Chem. Soc.* **2010**, *132*, 6923−6925.
(28) Makiura, R.; Motoyama, S.; Umemura, Y.; Yamanaka, H.; Sakata, O.; Kitagawa, H. Surface Nano-Archtechture of a Metal-Organic Framework. *Nat. Mater.* **2010**, *9*, 565−571.
(29) Fukuzumi, S.; Ohkubo, K.; Imahori, H.; Shao, J.; Ou, Z.; Zheng, G.; Chen, Y.; Pandey, R. K.; Fujitsuka, M.; Ito, O.; Kadish, K. M. Photochemical and Electrochemical Propertoes of Zinc Chlorin-C_{60} Dyad as Compared to Coresponding Free-Base Chlorin-C_{60}, Free-Base Chlorin-C_{60}, and Zinc Poorphyrin-C_{60} Dyads. *J. Am. Chem. Soc.* **2001**, *123*, 10676−10683.
(30) Fukuzumi, S.; Yoshida, Y.; Urano, T.; Suenobu, T.; Imahori, H. Etremely Slow Long-Range Electron Transfer reactions Across Zeolite-Solution Interface. *J. Am. Chem. Soc.* **2001**, *123*, 11331−11332.
(31) Li, H.; Choi, J.; Nakanishi, T. Optoelectronic Functional Materials Based on Alkylated-π Molecules: Self-Assembled Architechtures and Nonassembled Liquids. *Langmuir* **2013**, *29*, 5394−5406.
(32) Zhang, B. W.; Ochi, K.; Fujiki, M.; Naito, M.; Ishikawa, M.; Kaneto, K.-I.; Takashima, W.; Saeki, A.; Seki, S. Programmed high-Hole-Mobility Supramolecular Polymers from Disk-Shaped Molecules. *Adv. Funct. Mater.* **2010**, *20*, 3941−3947.
(33) Ishikawa, M.; Fujiki, M.; Naito, M. Highly Organized Phtalocyanine Assembly onto Gold Surface through Spontaneous Polymerization. *Chem. Lett.* **2007**, *36*, 304−305.
(34) Okada, S.; Segawa, H. Substituent-Control Exciton in J-Aggregates of Protonated Water-Insoluble Porphyrins. *J. Am. Chem. Soc.* **2003**, *125*, 2792−2796.
(35) Zhao, W.; Tong, B.; Pan, Y.; Shen, J.; Zhi, J.; Shi, J.; Dong, Y. Fabrication, Electrochemical, and Optoelectronic Properties Layer-by-Layer Films Based on (Phthalocyaninato)ruthenium(II) and Trir-uthenium Dodecacarbonyl Bridged by 4,4′-Bipyridine as Ligand. *Langmuir* **2009**, *25*, 11796−11801.
(36) Oekermann, T.; Schlettwein, D.; Jaeger, N. I. Charge Transfer and Recombination at Electrodes of Molecular Semiconductors Investigated by Intensity Modulated Photocurrent Spectroscopy. *J. Phys. Chem. B* **2001**, *105*, 9524−9532.
(37) Imahori, H.; Fukuzumi, S. Porphyrin- and Fullerene-Based Molecular Photovoltaic Devices. *Adv. Funct. Mater.* **2004**, *14*, 525−536.
(38) Schlettwein, D.; Kaneko, M.; Yamada, A.; Woehrle, D.; Jaeger, N. I. Light-Induced Dioxygen Reduction at Thin Film Electrodes of Various Porphyrins. *J. Phys. Chem.* **1991**, *95*, 1748−1755.
(39) Qu, S.; Li, M.; Xie, L.; Huang, X.; Yang, J.; Wang, N.; Yang, S. Noncovalent Functionalization of Graphene Attaching [6,6]-Phenyl-C61-butyric Acid Methyl Ester (PCBM) and Application as Electron Extraction Layer of Polymer Solar Cells. *ACS Nano* **2013**, *7*, 4070−4081.

DOI: 10.1021/acsami.5b04646
ACS Appl. Mater. Interfaces 2015, 7, 19098−19103

(40) Bard, A. J.; Faulkner, L. R. *Electrochemical Methods: fundamentals and applications*, 2nd ed.; John Wiley and Sons, Inc.: New York, 2001.
(41) Huang, Y.; Kramer, E. J.; Heeger, A. J.; Bazan, G. C. Bulk Heterojunction Solar Cells: Morphology and Performance Relationship. *Chem. Rev.* **2014**, *114*, 7006−7043.
(42) Matsuo, Y.; Sato, Y.; Niinomi, T.; Soga, I.; Tanaka, H.; Nakamura, E. Columnar Structure in Bulk Heterojunction in Solution-Processable Three-Layered p-i-n Organic Photovoltaic Devices Using Tetrabenzoporphyrin Precursor and Silylmethyl[60]fullerene. *J. Am. Chem. Soc.* **2009**, *131*, 16048−16050.
(43) Tanaka, H.; Abe, Y.; Matsuo, Y.; Kawai, J.; Soga, I.; Sato, Y.; Nakamura, E. An Amorphous Mesophase Generated by Thermal Annealing for High-Performance Organic Photovoltaic Devices. *Adv. Mater.* **2012**, *24*, 3521−3525.
(44) Wang, F.; Seo, J. H.; Li, Z.; Kvit, A. V.; Ma, Z.; Wang, X. Cl-Doped ZnO Nanowires with Metallic Conductivity and Their Application for High-performance Photoelectrochemical Electrodes. *ACS Appl. Mater. Interfaces* **2014**, *6*, 1288−1293.
(45) Chang, C.-Y.; Wu, C.-E.; Chen, S.-Y.; Cui, C.; Cheng, Y.-J.; Hsu, C.-S.; Wang, Y.-L.; Li, Y. Enhanced Performance and Stability of a Polymer Solar Cell by Incorporation of Vertically Aligned Fullerene Nanorods. *Angew. Chem., Int. Ed.* **2011**, *50*, 9386−9390.

DOI: 10.1021/acsami.5b04646
ACS Appl. Mater. Interfaces 2015, 7, 19098−19103